

# Optical and Radioiodinated Tethered Hsp90 Inhibitors Reveal Selective Internalization of Ectopic Hsp90 in Malignant Breast Tumor Cells

Jared J. Barrott,<sup>1</sup> Philip F. Hughes,<sup>1</sup> Takuya Osada,<sup>2</sup> Xiao-Yi Yang,<sup>2</sup> Zachary C. Hartman,<sup>2</sup> David R. Loiselle,<sup>1</sup> Neil L. Spector,<sup>3</sup> Len Neckers,<sup>6</sup> Narasimhan Rajaram,<sup>4</sup> Fangyao Hu,<sup>4</sup> Nimmi Ramanujam,<sup>4</sup> Ganesan Vaidyanathan,<sup>5</sup> Michael R. Zalutsky,<sup>5</sup> H. Kim Lyerly,<sup>2</sup> and Timothy A. Haystead<sup>1,\*</sup>

<sup>1</sup>Department of Pharmacology and Cancer Biology

<sup>2</sup>Department of Surgery

<sup>3</sup>Department of Medicine

<sup>4</sup>Department of Biomedical Engineering

<sup>5</sup>Department of Radiology

Duke University, Durham, NC 27710, USA

<sup>6</sup>Urologic Oncology Branch, Center for Cancer Research, National Cancer Institute, 9000 Rockville Pike Bldg. 10/CRC, Room 1-5940, Bethesda, MD 20892-1107, USA

\*Correspondence: [hayst001@dm.duke.edu](mailto:hayst001@dm.duke.edu)

<http://dx.doi.org/10.1016/j.chembiol.2013.08.004>

## SUMMARY

Inhibitors of heat-shock protein 90 (Hsp90) have demonstrated an unusual selectivity for tumor cells despite its ubiquitous expression. This phenomenon has remained unexplained, but could be influenced by ectopically expressed Hsp90 in tumors. In this work, we synthesized Hsp90 inhibitors that can carry optical or radioiodinated probes via a polyethyleneglycol tether. We show that these tethered inhibitors selectively recognize cells expressing ectopic Hsp90 and become internalized. The internalization process is blocked by Hsp90 antibodies, suggesting that active cycling of the protein occurs at the plasma membrane. In mice, we observed exquisite accumulation of the fluor-tethered versions within breast tumors at very sensitive levels. Cell-based assays with the radiolabeled version showed picomolar detection in cells that express ectopic Hsp90. Our findings show that fluor-tethered or radiolabeled inhibitors that target ectopic Hsp90 can be used to detect breast cancer malignancies through noninvasive imaging.

## INTRODUCTION

The current paradigm for detection and treatment of breast cancer is based on clinical evaluation and anatomic imaging, usually with mammography or (less commonly) breast MRI, followed by biopsy and surgery or surgery plus radiotherapy. Other imaging modalities, such as ultrasound and positron emission tomography (PET), are not routinely used for screening, although they have specific indications and potential (Smith et al., 2010). Although both mammography and MRI demonstrate excellent sensitivity for detecting tissue abnormalities, they lack sufficient

specificity to unequivocally distinguish malignant tissue from benign tissue (Esserman et al., 2009). The question remains as to whether premalignant molecular markers can be used noninvasively to detect aggressive cancers.

It is clear that anatomic changes are not the earliest cancer-related transformations. Instead, breast cells with malignant and lethal potential are characterized early on by activated oncogenic signaling nodes. These signaling nodes have been classified into a broad set of characteristics termed the “hallmarks of cancer” and are candidate molecular markers of malignant behavior (Hanahan and Weinberg, 2011). Unfortunately, these signaling nodes have been difficult to detect in vivo, particularly when they are confined to small clusters of cells, as in early-stage disease. To date, strategies to visualize these signals in vivo, such as using 18F-fluorodeoxyglucose (<sup>18</sup>FDG)-PET to detect increased glucose uptake, have not achieved the sensitivity or specificity required to appreciably improve breast cancer screening and diagnosis (Warning et al., 2011).

Heat-shock protein 90 (Hsp90) is a signaling node that could be exploited as a diagnostic molecular marker to distinguish malignant breast cells from normal tissues (Barrott and Haystead, 2013). Hsp90 plays an essential role in cellular homeostasis by chaperoning client proteins. Over 400 putative Hsp90 clients have been identified, and many of these regulate signaling pathways that govern cellular growth and differentiation (Echeverría et al., 2011; Moulick et al., 2011; Neckers et al., 2009; Samant et al., 2012; Vaughan et al., 2010). Hsp90 and its family members Grp94 and Trap-1 contain an N-terminal ATP-binding domain with ATPase activity that is necessary for cellular function (Tsutsumi et al., 2009). Hsp90 is regulated both translationally and posttranslationally, with the latter affecting both ATPase activity and intracellular location (Mollapour and Neckers, 2012). Direct evidence for Hsp90's participation in oncogenic protein folding/stability in vivo comes from studies with Hsp90 inhibitors that bind competitively to its ATP-binding domain, resulting in the degradation of its oncogenic clients (Chiosis et al., 2003; Csermely et al., 1998; Fadden et al., 2010). This phenomenon has also been demonstrated in

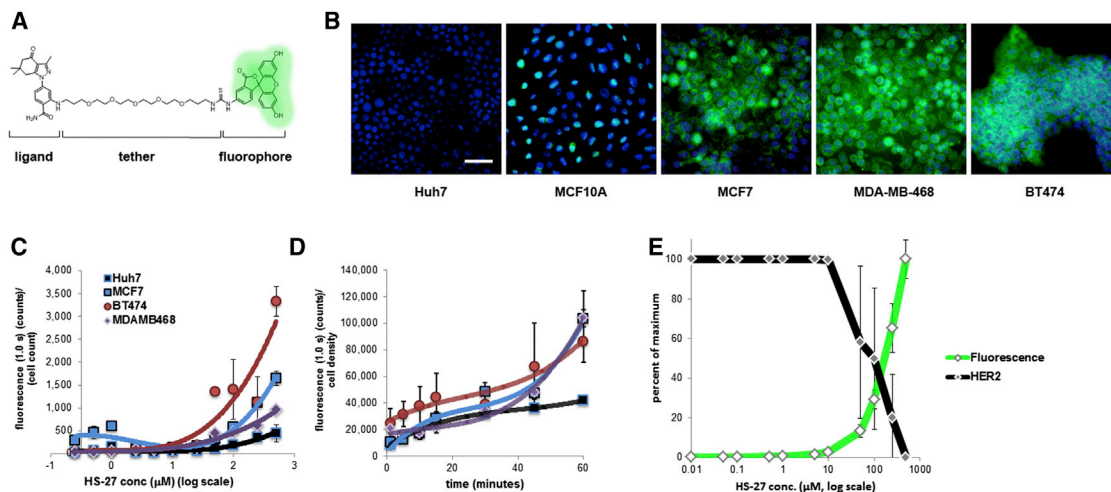


**Figure 1. Fluor-Tethered Hsp90 Inhibitors Label Breast Cancer Cell Lines**

(A) HS-27 structure given to illustrate the generic inhibitor design of the Hsp90 ligand conjugated to a linker series and tethered to a fluorophore. (B) HS-27, at 100  $\mu\text{M}$ , labels native Hsp90 in breast cancer cell lines and correlates with the established malignancy level of the cell lines. HS-27 does not label Huh7 cells under normal cell culture conditions. (C) In a dose titration curve of HS-27, cell lines become stratified at higher doses despite having approximately equivalent levels of total Hsp90 ( $n = 3$ ,  $\pm\text{SEM}$ ). (D) Time-course study showing that the kinetics of HS-27 (100  $\mu\text{M}$ ) uptake mirror the dose assay in terms of selectivity against breast cancer cell lines and the Huh7 cell line ( $n = 2$ ,  $\pm\text{SDM}$ ). (E) HS-27 on BT474 cells shows an inverse correlation between fluorescent uptake (green) and Her2 degradation (black);  $n = 2$ ,  $\pm\text{SDM}$ . Scale bar: 50  $\mu\text{m}$ . See also Figures S2 and S3.

human tumor biopsies from patients undergoing Hsp90 inhibitor therapy (Kim et al., 2009). To date, 17 different Hsp90 inhibitors that target Hsp90's ATP-binding site are in clinical development for multiple indications in cancer (Kim et al., 2009; Neckers and Workman, 2012; Trepel et al., 2010; Wang et al., 2010).

Recent studies have linked high expression of Hsp90 with poor prognosis in malignant breast tumors (Cheng et al., 2012; Pick et al., 2007). The role of Hsp90 in mediating malignant behavior may be the result of oncogene-driven factors that alter its normal cellular behavior (Whitesell and Lindquist, 2005). Hyperactivation is postulated to result in an increased affinity for ATP and Hsp90 inhibitors, and the expression of ectopic Hsp90 (Tsutsumi and Neckers, 2007; Tsutsumi et al., 2008). We reasoned that if oncogenically activated Hsp90 precedes malignant behavior in vivo, this could be used diagnostically (Eustace et al., 2004; McCreedy et al., 2010; Sims et al., 2011). We therefore developed a series of Hsp90 inhibitors tethered to fluorophores or radioiodine to detect Hsp90 in vivo. When injected into mice bearing human breast tumors, the fluorophore versions are exquisitely targeted to tumors. We show that this targeting is achieved through interactions with ectopic Hsp90, which undergoes active internalization along with the bound probes. This finding suggests new roles for Hsp90 in which the protein is not only trafficked to the plasma membrane but is also reinternalized.

## RESULTS

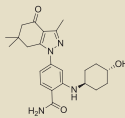
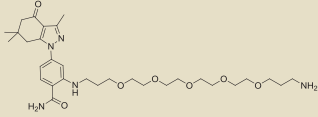
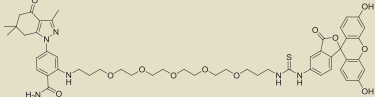
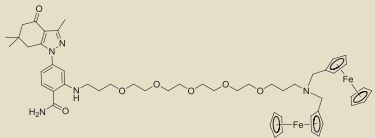
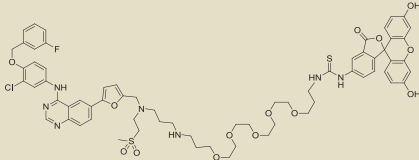
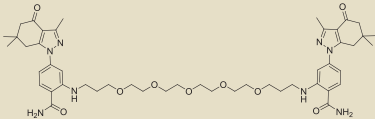
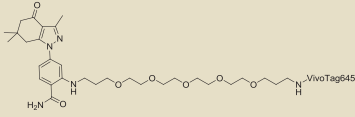
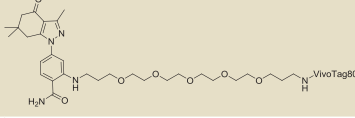
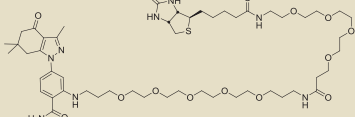
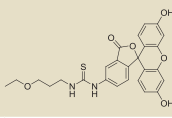
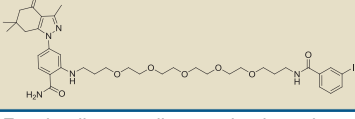
### Synthesis and Development of Probes that Selectively Target Ectopic Hsp90

We recently reported the development of a cleavable, tethered Hsp90 inhibitor and demonstrated its use as an affinity resin

(Hughes et al., 2012). When bound to the tethered ligand, Hsp90 could be recovered along with one of its established oncogenic clients, Her2, in a competitive manner. To extend our tethered ligand's utility, we synthesized several versions tethered to a variety of fluorophores and other molecules to facilitate the detection of Hsp90 in vivo (Figure 1A and Figure S1 available online; Table 1). In binding studies against immobilized ATP, the tethered inhibitors showed reduced affinity for native Hsp90 ( $K_d$  HS-27, 288 nM; HS-69, 49 nM; and HS-70, 42 nM) in comparison with the parent compound (HS-10, 3 nM; Table 1; Figure S2A; Fadden et al., 2010; Grenert et al., 1997). Despite some reduction in affinity, the addition of the tethered components was found to increase specificity by eliminating binding to Grp94 (Figure S2B). Previous work had also shown that the addition of the tether at the *ortho* position of the parent ligand reduced the specificity toward recombinant and native Trap-1 (Hughes et al., 2012). These findings suggest that the added steric bulk due to, e.g., the presence of the tether and added fluor, interferes with the ATP-binding site of Grp94 and Trap-1, but not Hsp90. We also observed a similar specificity when we added various nonfluorescent molecules, such as ferrocene, iodinated benzylamine, or an additional Hsp90 inhibitor, to the tethers to create a bifunctional inhibitor (Figure S2B; Table 1).

Next, we evaluated the specificity of the fluor probes in several transformed cell lines by fluorescent microscopy. Figure 1B shows that HS-27 is internalized by breast cancer cell lines, but, remarkably, not by Huh7 cells (a hepatocarcinoma cell line), even though the latter cell line has higher total cellular levels of Hsp90 as determined by immunoblotting (Figure S2C). Time-course and titration studies showed that HS-27 uptake is variable between breast lines in the following order: MCF10 < < MCF7 < MDA-MB-468 < BT474 (Figures 1C and

**Table 1. Hsp90 and Her2 Tethered Inhibitors**

Designation Name	Feature	Structure
HS-10	parent ligand	
HS-23	ligand + linker	
HS-27	ligand + FITC	
HS-32	bis-ferrocene	
HS-42	lapatinib + fluorescein	
HS-66	double ligand	
HS-69	ligand + nIR (645)	
HS-70	ligand + nIR (800)	
HS-96	ligand + biotin	
HS-105	FITC derivative w/o ligand	
HS-111	iodine-containing ligand	

Listed are the names, descriptive features, and structures of the compounds used in this study. For details regarding synthesis and analysis of the compounds, see [Figure S1](#).

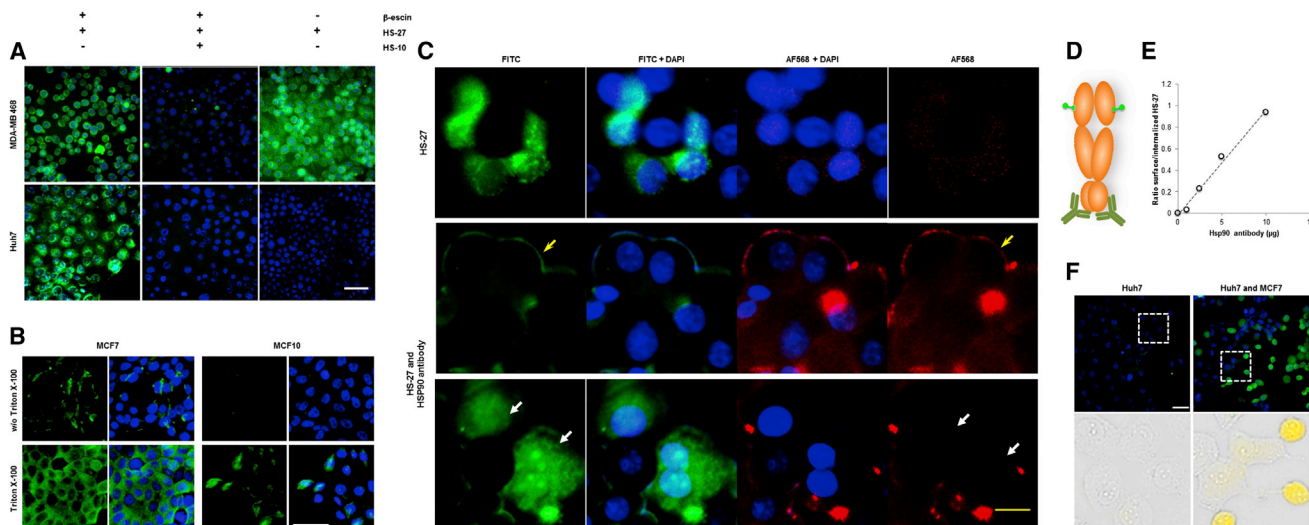


**Figure 2. HS-27 Labels Surface Hsp90 in Breast Cancer Cell Lines**

(A) HS-27 labels all of the cancer lines tested upon permeabilization with 5  $\mu$ M  $\beta$ -escin. Live-cell imaging demonstrates that the fluorescent signal is competed with a pretreatment of 10-fold excess of a nontethered Hsp90 inhibitor, HS-10.

(B) Fixed breast cancer cell lines are treated with or without a detergent (0.3% Triton X-100) and stained by immunofluorescence with an anti-Hsp90 antibody. Cells treated with Triton have intracellular pools that are labeled, whereas nonpermeabilized cells exhibit exclusive labeling of surface Hsp90.

(C) Antibody treatment prevents active internalization of Hsp90 and HS-27 in a dose-dependent manner. The first row shows incubation with HS-27 alone and denotes a single field observed with different filters. Rows 2 and 3 are separate fields of cells incubated with the antibody and HS-27. Row 2 demonstrates peripheral staining of Hsp90 (yellow arrow) by both the antibody (red) and HS-27 (green). Row 3 shows cells that are not labeled with the antibody and have internalized HS-27 (white arrows).

(D) Diagram of an Hsp90 dimer and the distant labeling of the anti-Hsp90 antibody and HS-27.

(E) The ratio of surface HS-27 and internalized HS-27 labeled cells plotted against the Hsp90 antibody titration;  $R^2 = 0.9903$ .

(F) Huh7 cells and Huh7-MCF7 cocultured cells treated with 100  $\mu$ M HS-27. White scale bars: 50  $\mu$ m; yellow scale bar: 20  $\mu$ m; black scale bar: 10  $\mu$ m.

See also [Figure S4](#).

1D). Interestingly, this uptake order correlates with the relative tumorigenicity of the cells to form tumors in severe combined immunodeficiency (SCID) mice (Neve et al., 2006). Analysis of Her2 levels in BT474 cells showed that once HS-27 is internalized, it is active as an Hsp90 inhibitor and uptake correlates with Her2 degradation (Figures 1E and S2D). Competition experiments with the untethered ligand HS-10 (Figure S2E) and comparisons with a control compound, fluorescein isothiocyanate (FITC)-tethered lapatinib (HS-42), demonstrate that HS-27 uptake and selectivity for the breast cells is Hsp90 dependent. In the case of HS-42, despite sharing a common fluorophore with HS-27, HS-42 was rapidly absorbed with identical kinetics in all cells tested, including Huh7 cells (Figures S3A–S3C). These findings show that the uptake of the two FITC-tethered inhibitors involves different mechanisms that are ligand dependent. As for HS-42, uptake may reflect binding to epidermal growth factor receptor, whereas for HS-27, the apparent mechanism is binding to ectopic Hsp90. This conclusion is consistent with other studies that linked extracellular Hsp90 with the metastatic potential of various tumor lines, including breast cancer cells (Koga et al., 2009; Tsutsumi and Neckers, 2007; Tsutsumi et al., 2008).

Additional support for the finding that the tethered Hsp90 inhibitors bind to ectopically expressed Hsp90 in breast cell lines came from observations made with the permeabilizing agents  $\beta$ -escin and Triton X-100. In the presence of  $\beta$ -escin, HS-27 entered all of the cells tested. To test whether HS-27 was nonspecifically labeling permeabilized Huh7 cells, we competed

HS-27 binding with HS-10, which blocked binding in both cell lines (Figure 2A). These data suggest that Huh7 cells do not express ectopic Hsp90, but they do contain an internal pool of Hsp90 that binds the inhibitor. We also observed other cell lines that were unable to internalize HS-27 without permeabilization, including lymphoma cells purified from patients with chronic lymphocytic leukemia, human peripheral blood mononuclear cells, or cultured fibroblasts.

Because of its polar nature, HS-27 would not be predicted to enter cells through passive diffusion, and the competition studies with HS-10 strongly argue that its internalization requires binding to Hsp90 expressed at the surface. Consistent with this hypothesis, anti-Hsp90 antibodies were found to selectively stain the surface of the more tumorigenic MCF7 cells compared with nontumorigenic MCF-10A cells (Figure 2B). Additionally, when live MCF7 cells were incubated with anti-Hsp90 antibodies in the presence of HS-27, the probe was retained at the plasma membrane and no longer internalized, as shown by costaining at the surface with the Hsp90 antibody (Figure 2C). A detailed examination of the stained fields shows that cells that are not colabeled with the antibody at the cell surface continue to internalize HS-27 (Figure 2C). Importantly, the Hsp90 antibody used in this experiment targets the C-terminal domain of the protein and does not interfere with the HS-27 binding at the N-terminal ATP-binding domain (Figure 2D). In antibody titration experiments, the retention of HS-27 at the surface correlates precisely with the antibody concentration. At 10  $\mu$ g/well of antibody, the

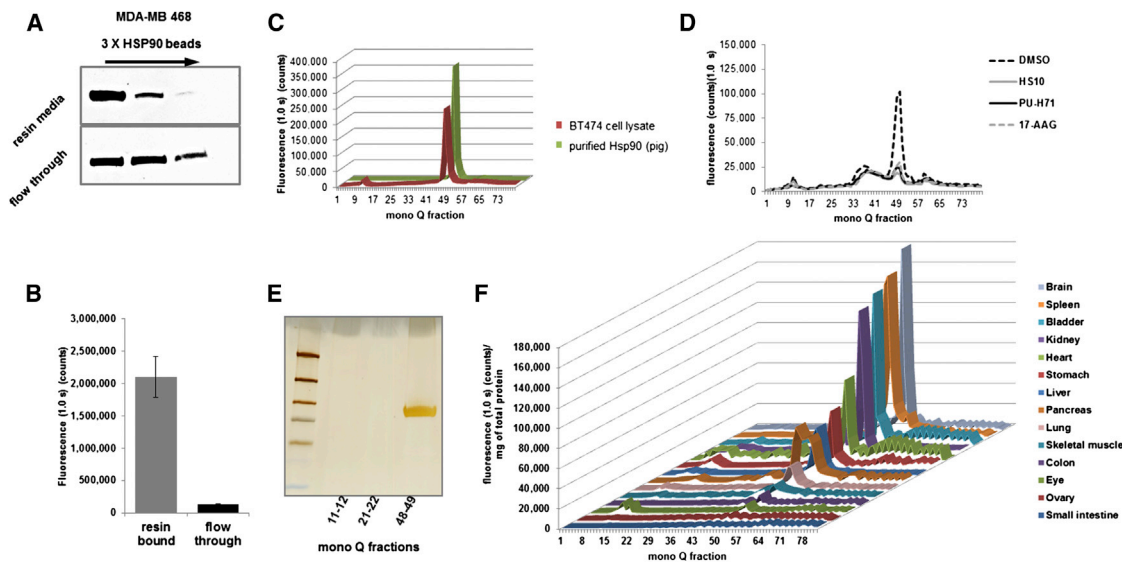


**Figure 3. HS-27 Binds to the Active Form of Hsp90 in Breast Cancer Cell Lines and Normal Mouse Tissues**

(A) Cell extracts from MDA-MB-468 were passed over immobilized Hsp90 ligand beads three times and the resin media and flowthrough were analyzed for total Hsp90 by immunoblotting. Hsp90 continued to be detected in the flowthrough even after depletion of the active form on the resin.

(B) The resin-bound extract and flowthrough were incubated with HS-27 and unbound probe was filtered away. Fluorescence was measured on a multilabel plate reader ( $n = 3$ ,  $\pm$ SEM, Student's  $t$  test,  $p < 0.005$ ).

(C) BT474 cell extracts treated with HS-27 ( $100 \mu\text{M}$ ) were compared with purified Hsp90 from a pig lactating mammary gland with HS-27 and separated on a mono Q anion-exchange column. Single fluorescent peaks were consistently observed peaking in the 49th fraction.

(D) MCF7 cells were pretreated with 10-fold excess of nonfluorescein Hsp90 inhibitors followed by  $10 \mu\text{M}$  HS-27. Cell lysates were harvested and separated on a mono Q anion-exchange column, and fluorescence from each fraction was measured.

(E) BT474 cell fractions corresponding to the fluorescent peak (48–49) and control fractions (11–12 and 21–22) were passed over the cleavable Hsp90 affinity resin to purify the protein and characterize it by gel electrophoresis. The silver-stained band was sequenced by mass spectrometry, which confirmed the presence of Hsp90.

(F) Mouse tissues were harvested from BALB/C mice and lysed tissues were incubated with HS-27. After the unbound probe was cleared away, the samples were analyzed by anion-exchange chromatography. Tissues were ordered from lowest- to highest-expressing tissues.

See also Figure S5.

ratio of cells that retained HS-27 at the surface to cells that internalized HS-27 was almost 1:1, whereas the ratio was 1:4 at an antibody treatment of  $2.5 \mu\text{g}/\text{well}$  (Figure 2E). Collectively, our data highlight a previously unrecognized pathway in which Hsp90 is not only trafficked to the membrane but is actively internalized. The internalization is likely not attributed to general pinocytosis that results in fusion with the lysosomes. Lysosomes have internal pH values of  $<6$ , and HS-27 consists of an Hsp90 inhibitor tethered to FITC, which loses its fluorescent properties below pH 6.5 (Figure S4A). Additionally, we failed to detect the colocalization of HS-27 with Rab5, a marker of early endosomes, by fluorescent microscopy or centrifugal enrichment of endosomes. We posit that the internalization mechanism of HS-27 is Rab5 independent.

Hsp90 is thought to be constitutively secreted only from tumor cells (Cheng et al., 2008; McCready et al., 2010; Wang et al., 2009). To detect the presence of secreted Hsp90, we added HS-27 to media derived from BT474, MCF7, and Huh7 cells, and removed the free probe by ultrafiltration. BT474 and MCF7 exhibited greater recovery of fluorescence compared with Huh7, which is consistent with the former cells actively secreting Hsp90 (Figure S4B). To examine whether extracellular Hsp90 is sufficient to facilitate HS-27 uptake into Huh7 cells, MCF7 cells were cocultured with Huh7 cells and incubated with HS-27.

Figure 2F shows that the presence of locally secreted Hsp90 from MCF7 cells is not sufficient to promote subsequent reuptake into the Huh7 cells. This suggests that Huh7 cells lack the necessary machinery for active internalization of HS-27 bound to Hsp90.

### Fluor-Tethered Hsp90 Inhibitors Are Selective for Active Hsp90 In Vitro

Our probes can discriminate between various cell lines, but recent data suggest that there are distinct populations of active and inactive Hsp90 within a given cell (Kamal et al., 2003; Moullick et al., 2011). To test whether our probes could also discriminate between these cellular pools in vivo, we first isolated these pools using affinity chromatography. Briefly, cell extracts from BT474 cells were repetitively passed over virgin Hsp90 affinity resins. The “active pool” binds and the “nonactive pool” flows through the resin (Figures 3A and 3B; Hughes et al., 2012). Once it was separated, Hsp90 from the resin-bound pool demonstrated 15.5-fold higher HS-27 binding compared with inactive Hsp90 in the flowthrough. To further characterize the HS-27-bound active pool of Hsp90, we separated either purified Hsp90 (from lactating pig mammary gland) or BT474 cell extracts incubated with HS-27 by micro-anion-exchange chromatography. In the extracts from the BT474 cells, we expected to

see multiple column fractions with fluorescence in the breast cancer cell extract, consistent with multiple interactions of active Hsp90 with its respective client proteins. However, in all cases, only a single peak of fluorescence was observed, which correlated precisely with the migration of purified pig mammary Hsp90 bound to HS-27 (Figure 3C). Furthermore, we competed the binding of HS-27 with three structurally distinct Hsp90 inhibitors: HS-10, PUH71, and 17-AAG. MCF7 cells were incubated with the nonfluorescein Hsp90 inhibitors followed by HS-27. Equal competition was observed with the three Hsp90 inhibitors compared with the DMSO control treatment (Figure 3D). The presence of Hsp90 in the single peak was confirmed after column fractions containing fluorescence were passed over the cleavable Hsp90 affinity resin followed by SDS-PAGE, silver staining, and mass spectrometry (Figure 3E). Collectively, these biochemical data strongly argue that the only intracellular target for HS-27 is an active pool of Hsp90 that is largely devoid of client proteins. These data are consistent with previous work by our laboratory using Hsp90 small-molecule affinity resins, which showed that the ligand-bound form is not associated in vivo with multiple clients as was previously thought (Hughes et al., 2012).

We next explored whether the probes could be used to measure acute activation of Hsp90 in cells in response to heat stress. We show that heat stress produces a consistent 1.2-fold increase in fluorescence eluting in the 49th fraction (Figures S5A and S5B). We then examined whether we could use the probe to quantify the amount of activated Hsp90 distributed in normal tissues by adding HS-27 to homogenized mouse tissue extracts and then fractionating the tissue extracts chromatographically. We show that the homogenized tissues contain diverse levels of active Hsp90, which also elutes as a single peak (Figure 3F). The significance of these observations is that nontumorigenic tissues contained an active pool of Hsp90, and the levels were especially high in brain, spleen, bladder, and kidney. Irrespective of this finding, only intact cells expressing ectopic Hsp90 are capable of internalizing the fluor-tethered inhibitors. We suggest that malignant tumor cells express ectopic Hsp90 and that this pool of Hsp90 can be used to discriminate between malignancies in vivo and normal tissues or more benign tumor cells. We also conclude that although the probe can reflect the tumorigenic state, the drug-bound version must have a low affinity for client proteins, in stark contrast to the conclusions reported by others (Moulick et al., 2011).

### Fluor-Tethered Hsp90 Inhibitors Specifically Target Human Breast Tumors in Mice

To test whether fluor-tethered Hsp90 inhibitors can be exploited to selectively visualize malignancies noninvasively, we injected the probes into mice bearing breast-tumor-derived xenografts. In MDA-MB-468 xenografts, we detected the tumor mass within 5 min postinjection with either HS-27 or the near-infrared (nIR) HS-69 and HS-70 versions in an IVIS kinetic fluorescent imager (Perkin-Elmer). In the case of HS-27, the tumor was clearly visible through the fur and could be discriminated from the natural background fluorescence normally observed at 520 nm (Figure 4A). With HS-27, an 8-fold increase over control tumors was consistently observed in mice that did not receive HS-27. With both nIR probes, we achieved a 150-fold increase at the

tumor site due to the low background signal at 660 nm or 800 nm (Figures 4B–4D and S6A). With nIR versions, postinjection, the probe was observed in the extremities (i.e., ears, nose, and paws) and eyes, reflecting the circulating unbound probe in the blood pool. This was not visible with the fluorescein versions because of the light scattering at 520 nm. Pharmacokinetic studies by various methods showed dose-dependent uptake of both the visible and nIR forms, peaking within the tumor mass by 30 min, and with a detectable signal remaining for up to 72 hr. To test whether the probes were binding to Hsp90 in vivo or just accumulating in the tumors because of a blood-pooling effect, the excised tumor lysates were fractionated chromatographically. As shown in Figure 3, a single major peak of fluorescence was observed that contained Hsp90 (Figure 4E).

Pharmacokinetic studies conducted over 96 hr by optical spectroscopy more elegantly confirmed selective uptake of the tethered inhibitors. In this in vivo approach, a spectral pen was placed at either the tumor site or an adjacent skin patch, and the fluorescence spectrum was measured from 500 to 620 nm. Figures 4F and 4G show the signature spectrum of fluorescein at the tumor site, but not at the adjacent skin sites, over a period of 6–24 hr postinjection. To rule out the possibility that the fluorescence measured in the tumor mass by IVIS imaging or the optical method was due to local blood pooling, we analyzed biopsied tissue sections by fluorescent microscopy (Figure 4H). Figure 4H shows discrete uptake of HS-27 within tumor cells. As a test of tumor selectivity in vivo, we simultaneously harvested tumor cells, splenocytes, and hepatocytes from SCID mice bearing MDA-MB-468 tumors over the course of 72 hr and analyzed the viable cells by flow cytometry for the presence of HS-27. Figure 4I shows specific uptake of the probe by tumor cells, but not by splenocytes or hepatocytes. The selectivity of HS-27 for tumor cells was further illustrated in pharmacokinetic studies. Mice were injected with HS-27 and its distribution and tissue uptake were analyzed by IVIS kinetic imaging or by fluorescent reading of tissue lysates. In all cases, the probe was retained within the tumor and there was no evidence of accumulation elsewhere (Figure 4J).

To ensure that the in vivo probe accumulation within the tumor was ligand dependent, we synthesized a control compound, HS-105. HS-105 consists of the fluorophore and tether minus the ligand. In affinity chromatography studies against Hsp90 bound to immobilized ATP, HS-105 showed no affinity for the protein, and therefore any tumor retention would be nonspecific (Figure S6B). Using IVIS kinetic imaging, we detected HS-27 through the skin in live animals at 1 hr, whereas HS-105 was below detection (Figure 5A). In more detailed necropsies, by 24 hr we found no trace of HS-105 by fluorescence, whereas HS-27 was still present within the tumor (Figures 5B and S6B). Next, we sought to quantify the amount of HS-27 that accumulated in the tumor by comparing the average radiant efficiency in the tumor with a standard curve of HS-27 concentrations measured by the IVIS kinetic imager (Figure 5C). We calculated that in a cohort of five mice, the mean accumulation of HS-27 was  $6.5 \mu\text{M} \pm 2.6$  (SEM). To test the utility of fluor-tethered Hsp90 inhibitors as a potential means of noninvasive, early tumor detection, we designed an assay to test the sensitivity of the nIR version, HS-70, in mice. MDA-MB-468 cells were treated ex vivo with HS-70 or control. A fixed number of cells were injected in an equal

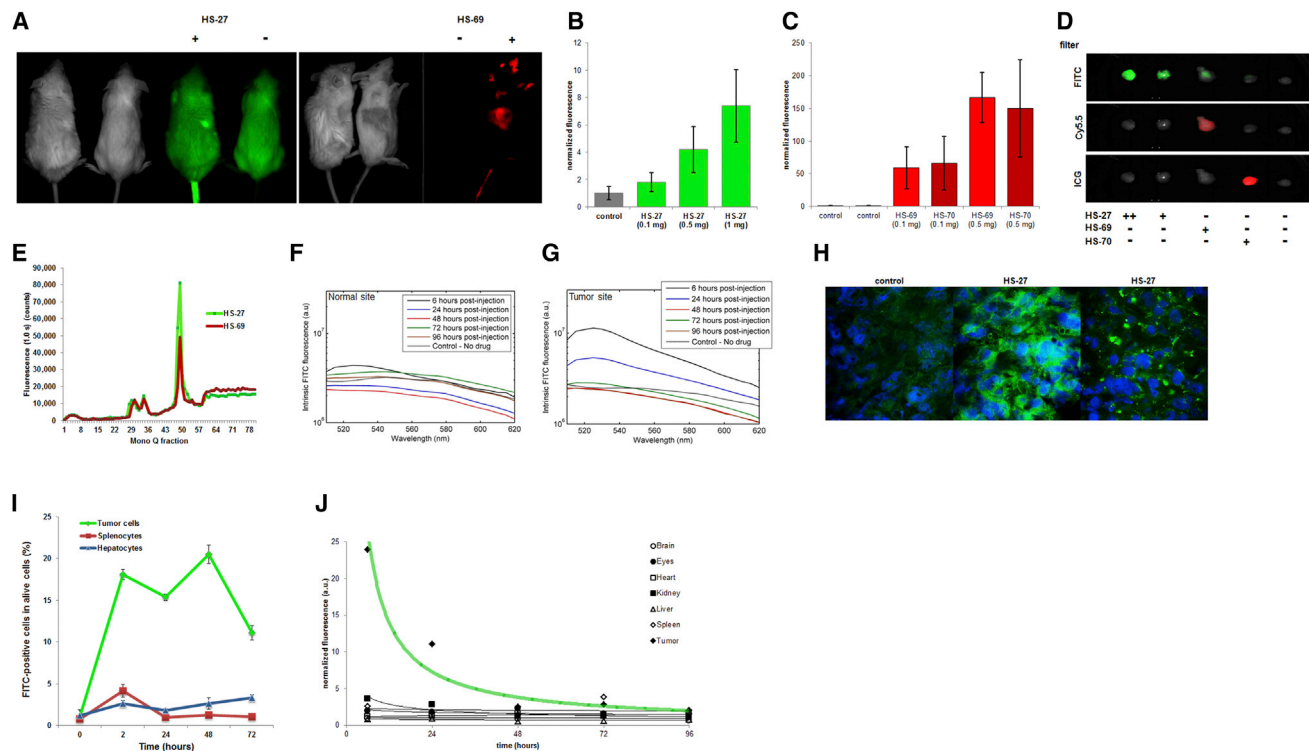


**Figure 4. Fluor-Tethered Hsp90 Inhibitors Target Human Breast Tumors in Mice**

(A) SCID mice bearing MDA-MB-468 xenografts in the right flank were injected with HS-27, HS-69, or saline and imaged using an IVIS kinetic imager. (B and C) HS-27 (B, green), HS-69 (C, red), and HS-70 (C, dark red) were injected with increasing doses into mice and tumors were excised ( $n = 2$ ,  $\pm$ SDM). (D) Examples of excised tumors from various treatments by IVIS. (E) Tumors from treated mice were excised, lysed, and fractionated on an anion-exchange column. (F and G) Fluorescence spectra measured from a normal site and the tumor at different times postinjection. Spectra are corrected for the effects of scattering and absorption from the tissue. Tumor shows signature FITC fluorescence at 6 hr and a reduced signal at 24 hr postinjection, which is also absent in the normal site. (H) Cryosections of biopsies taken from xenografts show the presence of the internalized probe within the tumor cells. (I) Flow cytometry of tumor cells, splenocytes, and hepatocytes over the course of 72 hr demonstrates the selectivity of the probe for tumor cells over the spleen and liver ( $n = 3$ ,  $\pm$ SEM). (J) Various tissues were excised from mice bearing tumors, injected with HS-27, and analyzed for fluorescence by IVIS imaging ( $n = 2$ ). See also [Figure S6](#).

volume into the right flank of SCID mice. We found that HS-70 could be detected at as little as 100,000 cells ([Figures 5D and 5E](#)). Current imaging approaches by MRI or PET/CT are estimated to reliably detect tumor masses at  $1 \text{ cm}^3$  with an estimated cell mass of  $\sim 10$  million cells ([Ide and Suzuki, 2005; Schoder and Gonen, 2007](#)). By these criteria, 100,000 cells would suggest that nIR probes could theoretically detect masses as low as  $0.01 \text{ cm}^3$ .

Based upon our findings with the nIR probes, an obvious application for early malignancy detection would be surface tumors in which upregulation of Hsp90 has been indicated, such as head and neck, colorectal, bladder, and melanoma ([Wang et al., 2010; Yin et al., 2010](#)). Because nIR probes are limited to 3–4 cm in tissue depth, to enable whole-body imaging, we investigated an alternative approach using tethered Hsp90 inhibitors capable of carrying the radioisotope  $^{125}\text{I}$  ( $^{125}\text{I}$ HS-111). Picomolar amounts of  $^{125}\text{I}$ HS-111 were added to MCF7, BT474, or Huh7 cells, and as observed with the fluor versions, the breast cancer cells exhibited greater uptake compared with the Huh7 cells ([Figure S6C](#)). Uptake of  $^{125}\text{I}$ HS-111 into MCF7 and Huh7

cells was then characterized after chromatographic fractionation, and the probe was detected by its radioactivity. As observed with the fluor-tethered versions, in MCF7 cells the majority of the radioactivity migrated as a single peak, in stark contrast to Huh7 cells, which showed no peak recovery ([Figure 5F](#)). Importantly, the signal in MCF7 cells was effectively competed by the free ligand, HS-10 ([Figure 5G](#)). As with the fluor versions,  $\beta$ -escin permeabilization of Huh7 cells permitted labeling of Hsp90 with  $^{125}\text{I}$ HS-111 in a competitive manner ([Figures 5H and 5I](#)).

Importantly, HS-111 behaves similarly to the fluor-tethered versions in terms of its selectivity toward the breast cancer cell lines, and entry into these cells also clearly requires active internalization through binding to ectopic Hsp90. Interestingly, HS-111 is more potent than the fluor versions in Her2 knock-down assays, suggesting faster kinetics of internalization, and performed most similarly to HS-10, the parent untethered compound. This is likely due to the differences in added steric bulk of the attached imaging moieties. HS-111 consists of a benzylamide moiety of 121.1 Da, whereas HS-27 carries a bulky

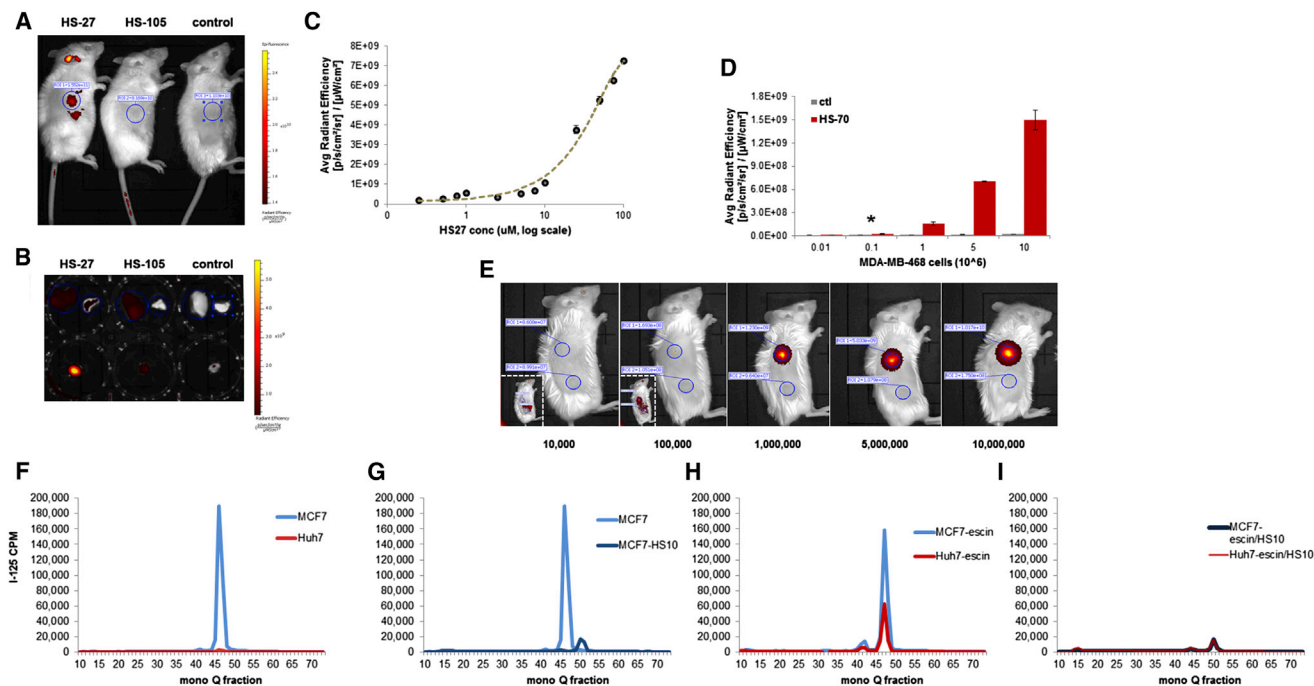


**Figure 5. Tumor Detection Limits and Specificity Using Optical or Radioiodinated Tethered Hsp90 Inhibitors**

(A) IVIS kinetic images (1 hr postinjection) of mice bearing MDA-MB-468 tumors and injected with HS-27, HS-105, or control. Liver (L) and lung (R) are shown in the top rows and the tumors are shown in the bottom row.

(B) IVIS kinetic images (24 hr postinjection) of excised tissues from SCID mice bearing MDA-MB-468 tumors and injected with HS-27, HS-105, or control. Liver (L) and lung (R) are shown in the top rows and the tumors are shown in the bottom row.

(C) IVIS average radiant efficiency plotted against the concentration of HS-27; mean  $\pm$  SEM.

(D and E) IVIS average radiant efficiency of live mice injected with MDA-MB-468 cells treated ex vivo with HS-70 or control; mean  $\pm$  SDM.

(F–I) MCF7 and Huh7 cells treated with [ $^{125}$ ]HS-111 and cell lysates fractionated on a mono Q anion-exchange column: (F) MCF7 and Huh7 cells under normal conditions, (G) MCF7 cells treated with and without HS-10, (H) MCF7 and Huh7 cells treated with  $\beta$ -escin, and (I) MCF7 and Huh7 cells treated with  $\beta$ -escin and HS-10. \* $p = 0.0424$ .

See also Figure S6.

fluorescein moiety of 389.0 Da. Similarly, a lower rate of entry was observed with HS-96, a biotin-tethered Hsp90 inhibitor that is considered to not passively diffuse across cell membranes (Figure S2D). These data strongly suggest that one can readily manipulate the entry rate of tethered inhibitors into cells expressing ectopic Hsp90 by changing the properties of the tethered imaging moiety. The finding that tethered inhibitors with structurally diverse imaging prosthetic groups only enter cells expressing ectopic Hsp90, and at variable rates, excludes the possibility that the entry of the tested probes occurs through simple diffusion.

## DISCUSSION

Our data show that an important frontline cancer target, Hsp90, can be exploited through its role in the oncogenic process as a diagnostic marker for real-time imaging of metastatic status. This observation represents somewhat of a paradigm shift in the way we currently view cutting-edge therapeutic targets such as Hsp90, and the concept could be extended to other therapeutic targets. Tethered Hsp90 inhibitors as imaging agents potentially add an element of diagnostic detail that cannot be garnered from expression analysis or deep-sequencing techniques. Specifically for Hsp90, these tech-

niques do not measure the activation state of the protein or its localization, two important parameters that have been linked to disease progression in breast cancer (Moulick et al., 2011; Tsutsumi and Neckers, 2007). The urgency to exploit this approach is made more relevant by the recent landmark studies of Gerlinger et al. (2012), who demonstrated the degree to which tumors exhibit phenotypic heterogeneity, even within the same tumor. Because expression analysis and deep sequencing reveal only a fraction of a tumor's global heterogeneous expression pattern at a single time point, these approaches have a limited ability to stratify and diagnose tumors. However, because tumor growth requires the continued activation of signal pathways, the development of fluor-tethered and other imaging inhibitors that target proteins such as Hsp90, or constitutively activated oncogenes such as Her2, could provide an alternative strategy to stratify disease progression more accurately through real-time, noninvasive imaging.

If expression of ectopic Hsp90 signifies metastatic behavior in vivo, the fluor- or [ $^{125}$ ]carrying tethered Hsp90 inhibitors could be used in conjunction with current biopsy practice to diagnose aggressive tumors. This would simply involve histological examination to determine probe uptake following micro-dose administration prior to the biopsy procedure. Moreover, noninvasive whole-body PET imaging could be employed with



<sup>124</sup>I-containing tethered versions. The PET-based approach is attractive because it would allow one to determine the fate and distribution of the tethered inhibitor in all tissues simultaneously and in real time. If PET analysis of a <sup>124</sup>I-carrying version showed highly selective targeting to the tumor in an individual, one could proceed to a <sup>131</sup>I version (which emits cytotoxic  $\beta$  particles) with the goal of achieving complete body-wide tumor ablation without unwanted damage in normal tissues. The known micromolar accumulations of Hsp90 inhibitors (5–20  $\mu$ M; Fadden et al., 2010) within tumors, as well as established protocols for the treatment of thyroid cancers with <sup>131</sup>I, should help accelerate the development of such treatment strategies.

The importance of ectopically expressed Hsp90 in the metastatic process has been established in a variety of ways, including the use of a functional proteomic screen (Eustace et al., 2004) and a non-cell-permeable form of geldanamycin (DMAG-N-oxide) and anti-Hsp90 antibodies, both of which block cellular migration in metastatic tumor lines (Koga et al., 2009; Sidera et al., 2011; Stellas et al., 2010; Tsutsumi et al., 2008; Xu et al., 2005). The observation that fluor-tethered versions are selectively internalized by binding to ectopically expressed Hsp90 has revealed previously unrecognized roles for the protein in vivo. Although the expression of surface Hsp90 appears to be connected to cell migration and metastasis, the molecular mechanism by which ectopic Hsp90 signals to the tumor cell to promote these events is not known. Both migration to the surface and reinternalization of Hsp90 could involve low-copy clients, which may provide a means of signaling that promotes cellular migration and metastasis. This conclusion is supported by the finding that anti-Hsp90 antibodies blocked reinternalization of Hsp90, as reflected by inhibition of HS-27 uptake into MCF7 cells. Irrespective of the roles played by ectopic Hsp90 in metastatic progression, the knowledge that the protein is reinternalized could be exploited to improve the safety margins of existing Hsp90 therapeutics or selectively deliver chemotoxic payloads to tumor cells. In contrast to other cancer therapeutics, Hsp90 inhibitors are generally well tolerated by humans, although some dose-limiting side effects (e.g., night blindness) have been observed (Zhou et al., 2012).

## SIGNIFICANCE

**To many researchers, the notion that inhibition of Hsp90 can be used therapeutically at all may seem paradoxical. After all, Hsp90 is thought to represent 1%–3% of the expressed protein in most cells. This paradox is even more extraordinary in the light of the biochemical studies presented herein, including the finding that extracts from normal tissues contain considerable levels of active Hsp90. Various explanations have been offered in the past concerning the extraordinary selectivity of various Hsp90 inhibitors for tumor cells, including the idea that tumor cells express an oncogenically activated form of Hsp90 with a higher affinity for Hsp90 inhibitors (Kamal et al., 2003). Our results suggest that the expression of ectopic Hsp90 may play a substantial role in the entry of Hsp90 inhibitors in general. This finding also suggests**

**that in addition to tumor imaging, it may be possible to extend the therapeutic window of Hsp90 inhibitors by developing a range of molecules that do not passively diffuse across the plasma membrane, and can only enter cells expressing ectopic Hsp90.**

## EXPERIMENTAL PROCEDURES

### Studies with HSP90 Antibodies

MCF7 and MCF10A cells were cultured and fixed in wells with 4% paraformaldehyde/PBS. The cells were successively incubated in blocking solution (5% goat serum, 0.2% Na Azide, PBS) with or without 0.3% Triton X-100 for 1 hr. After blocking with or without the detergent, the cells were incubated with a polyclonal antibody for HSP90 at 1:100 (sc-7947; Santa Cruz Biotechnology). The cells were sequentially incubated with a goat-anti-rabbit Alexa Fluor 488-conjugated antibody at 1:1,000 (A-11008; Life Technologies). Cells were imaged with an Olympus IX 71 epifluorescence microscope. To evaluate ectopic expression of HSP90, HSP90 antibody was incubated with live MCF7 cells (2.5 hr), and then 100 nM of HS-27 was added. Concurrently, the cells were stained with DAPI and goat-anti-rabbit Alexa Fluor 568 secondary antibody (A11011; Life Technologies) at 1:1,000 and incubated for 1 hr at 37°C. The cells were washed in PBS and imaged with the Olympus IX 71 epifluorescence microscope. The ratios of cells that retained HS-27 at the cell periphery to cells that internalized HS-27 were calculated and plotted against the antibody mass.

### Anion-Exchange Chromatography

Samples from either cell or tissue lysates underwent buffer exchange using 30K filter devices. Lysis buffers were exchanged for 25 mM Tris-HCl and 1 mM dithiothreitol (DTT). Samples were centrifuged (13,000 rpm, 10 min) and then passed through a 0.2  $\mu$ m syringe filter. Next, the supernatants were loaded onto a Pharmacia mono Q anion-exchange SMART column (0.1  $\times$  1.0 cm) that had been equilibrated in 25 mM Tris-HCl, 1 mM DTT buffer, pH 7.4, as previously described (Ray and Haystead, 2003). The column was eluted using a linear salt gradient over 80 min (100  $\mu$ l/min) to 1 M NaCl in the same buffer. Samples were fractionated into an opaque plate that was read for fluorescence on a multilabel plate reader. Peak fractions of fluorescence were passed over a cleavable affinity resin to purify Hsp90 as previously described (Hughes et al., 2012).

### IVIS Kinetic Mouse Imaging

All protocols involving the use of mice were approved beforehand by the IACUC at Duke University and strictly adhered to throughout the studies. SCID mice bearing MDA-MB-468 tumors were anesthetized with ketamine. Mice received tail vein injections or abdominal injections and were imaged postinjection at the indicated times using an IVIS kinetic imager (Caliper Life Science) as part of the Optical Molecular Imaging and Analysis shared resource at the Duke Cancer Institute. The following filters were used for the corresponding small-molecule inhibitors (emission/excitation): HS-27 (468/GFP), HS-105 (468/GFP), HS-69 (640/Cy5.5), and HS-70 (745/ICG).

### Tissue Harvest and Analysis

Mouse tissues (blood, brain, eyes, heart, kidney, liver, lung, spleen, and tumor) were obtained immediately postmortem. With the exception of the blood, the tissues were rinsed in PBS and blotted, followed by image analysis using the IVIS kinetic imager. Tissues were stored on dry ice or at  $-80^{\circ}$ C. For analysis of tissue lysates using SMART mono Q fractionation and the multilabel fluorescent reader, tissues were dounced in mono Q buffer (25 mM Tris-HCl, 1 mM DTT). We centrifuged the samples and transferred supernatants to be analyzed for fluorescence and protein concentration.

### Fluorescence Spectroscopy of Drug Uptake

SCID mice bearing MDA-MB-468 tumors were anesthetized with ketamine and received tail-vein drug injections. Using an optical spectroscopy instrument and a fiber-optic probe, we measured the fluorescence spectrum of the FITC-conjugated drug in vivo at 6, 24, 48, 72, and 96 hr postinjection (Brown et al., 2009). For optical spectroscopy, we illuminated tissues using the light of interest and analyzed the reflected light to study the morphology

and biochemical composition of the underlying tissue. The pen-shaped fiber-optic probe had a diameter of ~2 mm and was placed in gentle contact with the tumor or adjacent normal site. Incident light at 490 nm corresponding to FITC excitation was delivered through the probe into the tissue and the resulting longer-wavelength fluorescent light was collected. Although 490 nm does not correspond to maximal absorption by FITC, this wavelength was used to minimize fluorescent contributions from flavin adenine dinucleotide (FAD), which fluoresces in the same wavelength range. Measured fluorescence spectra were corrected for tissue absorption and scattering using an intrinsic fluorescence recovery model described in the literature (Palmer and Ramanujam, 2008). Briefly, the model calculates the tissue optical properties that are a function of light scattering and absorption, and uses these properties to correct distortions in the measured fluorescence. The intrinsic fluorescence model has been shown to recover fluorophore concentrations accurately in tissue-mimicking phantoms (Liu et al., 2012). In addition, the intrinsic fluorescence calculated with this model has been used to monitor intratumor drug concentrations in vivo and shown to be strongly correlated with concentrations measured by high-performance liquid chromatography (Palmer et al., 2010). Because optical spectroscopy measures wavelength-dependent fluorescence, the background fluorescence can be accurately measured prior to injection. This allows one to monitor the fluorophore concentration in vivo and determine when the fluorescent tether has cleared from the tumor.

#### Active Hsp90 Depletion Using Affinity Resin Chromatography

MDA-MB-468 cell lysate was diluted to 1 mg/ml in low-stringency wash buffer and 1 ml was added to 1 ml of the Hsp90 affinity resin at 50% slurry. For three consecutive washes, fresh resin was used and 25  $\mu$ l of flowthrough (<3%) was set aside for flowthrough analysis. The resin was washed thoroughly with low-stringency wash buffer and then Hsp90 was eluted off with 10% SDS. Both flowthrough and resin samples were characterized by one-dimensional SDS-PAGE and silver staining. In a separate experiment, flowthrough and resin samples were incubated with 100 nM HS-27 and then washed using a 10K kDa filter. Samples were concentrated and analyzed on a multilabel plate reader for fluorescence.

#### Ex Vivo Cell Treatment and Injection into Mice

MDA-MB-468 cells were treated with 5  $\mu$ M  $\beta$ -escin for 5 min. Cells were harvested and treated with either 10  $\mu$ M HS-70 or PBS. The cells were counted and aliquots of 10 million to 10,000 cells were made in 200  $\mu$ l of saline. SCID mice were anesthetized with ketamine and received two flank injections of the treated cells and the control cells. Mice were imaged using the IVIS kinetic imager and the average radiant efficiency was measured.

#### <sup>125</sup>I-Labeled Hsp90 Inhibitor Treatment of Cells

Cells were permeabilized by treatment with 5  $\mu$ M  $\beta$ -escin for 5 min. Competition experiments were performed by treating the cells with 1  $\mu$ M of HS-10 for 5 min before exposing them to [<sup>125</sup>I]HS-111.  $\beta$ -escin and HS-10 were washed away and the cells were then incubated in 5 ml of medium with the [<sup>125</sup>I]HS-111, which had ~10  $\mu$ Ci of activity per 10 cm dish of cells, for 45 min. The cells were washed extensively with PBS and then lysed on an ethanol/dry ice bath and harvested in 25 mM Tris buffer and centrifuged. Supernatants were fractionated on a Pharmacia mono Q anion-exchange SMART column, and fractions were counted using a PerkinElmer 1480 Wizard 3 gamma counter for 30 s per fraction sample.

For further details regarding the materials and methods used in this work, see [Supplemental Experimental Procedures](#).

#### SUPPLEMENTAL INFORMATION

Supplemental Information includes Supplemental Experimental Procedures and six figures and can be found with this article online at <http://dx.doi.org/10.1016/j.chembiol.2013.08.004>.

#### ACKNOWLEDGMENTS

This work was funded by NIH grants 1R01-AI089526-01 and 1R01AI090644-01 to T.A.J.H. and a Department of Defense Transformative Vision Award to T.A.J.H., N.L.S., and H.K.L. There is a patent-pending application by P.F.H.

and T.A.H. for several of the small-molecule inhibitors listed in this work. Reagents are available upon request.

Received: June 3, 2013

Revised: July 18, 2013

Accepted: August 10, 2013

Published: September 12, 2013

#### REFERENCES

- Barrott, J.J., and Haystead, T.A. (2013). Hsp90, an unlikely ally in the war on cancer. *FEBS J.* 280, 1381–1396.
- Brown, J.Q., Wilke, L.G., Geradts, J., Kennedy, S.A., Palmer, G.M., and Ramanujam, N. (2009). Quantitative optical spectroscopy: a robust tool for direct measurement of breast cancer vascular oxygenation and total hemoglobin content in vivo. *Cancer Res.* 69, 2919–2926.
- Cheng, C.F., Fan, J., Fedesco, M., Guan, S., Li, Y., Bandyopadhyay, B., Bright, A.M., Yerushalmi, D., Liang, M., Chen, M., et al. (2008). Transforming growth factor alpha (TGFalpha)-stimulated secretion of HSP90alpha: using the receptor LRP-1/CD91 to promote human skin cell migration against a TGFbeta-rich environment during wound healing. *Mol. Cell. Biol.* 28, 3344–3358.
- Cheng, Q., Chang, J.T., Geradts, J., Neckers, L.M., Haystead, T., Spector, N.L., and Lyster, H.K. (2012). Amplification and high-level expression of heat shock protein 90 marks aggressive phenotypes of human epidermal growth factor receptor 2 negative breast cancer. *Breast Cancer Res.* 14, R62.
- Chiosis, G., Lucas, B., Huezio, H., Solit, D., Basso, A., and Rosen, N. (2003). Development of purine-scaffold small molecule inhibitors of Hsp90. *Curr. Cancer Drug Targets* 3, 371–376.
- Csermely, P., Schnaider, T., Soti, C., Prohászka, Z., and Nardai, G. (1998). The 90-kDa molecular chaperone family: structure, function, and clinical applications. A comprehensive review. *Pharmacol. Ther.* 79, 129–168.
- Echeverría, P.C., Bernthaler, A., Dupuis, P., Mayer, B., and Picard, D. (2011). An interaction network predicted from public data as a discovery tool: application to the Hsp90 molecular chaperone machine. *PLoS ONE* 6, e26044.
- Esserman, L., Shieh, Y., and Thompson, I. (2009). Rethinking screening for breast cancer and prostate cancer. *JAMA* 302, 1685–1692.
- Eustace, B.K., Sakurai, T., Stewart, J.K., Yimlamai, D., Unger, C., Zehetmeier, C., Lain, B., Torella, C., Henning, S.W., Beste, G., et al. (2004). Functional proteomic screens reveal an essential extracellular role for hsp90 alpha in cancer cell invasiveness. *Nat. Cell Biol.* 6, 507–514.
- Fadden, P., Huang, K.H., Veal, J.M., Steed, P.M., Barabasz, A.F., Foley, B., Hu, M., Partridge, J.M., Rice, J., Scott, A., et al. (2010). Application of chemoproteomics to drug discovery: identification of a clinical candidate targeting hsp90. *Chem. Biol.* 17, 686–694.
- Gerlinger, M., Rowan, A.J., Horswell, S., Larkin, J., Endesfelder, D., Gronroos, E., Martinez, P., Matthews, N., Stewart, A., Tarpey, P., et al. (2012). Intratumor heterogeneity and branched evolution revealed by multiregion sequencing. *N. Engl. J. Med.* 366, 883–892.
- Grenert, J.P., Sullivan, W.P., Fadden, P., Haystead, T.A., Clark, J., Mimnaugh, E., Krutzsch, H., Ochel, H.J., Schulte, T.W., Sausville, E., et al. (1997). The amino-terminal domain of heat shock protein 90 (hsp90) that binds geldanamycin is an ATP/ADP switch domain that regulates hsp90 conformation. *J. Biol. Chem.* 272, 23843–23850.
- Hanahan, D., and Weinberg, R.A. (2011). Hallmarks of cancer: the next generation. *Cell* 144, 646–674.
- Hughes, P.F., Barrott, J.J., Carlson, D.A., Loiselle, D.R., Speer, B.L., Bodoor, K., Rund, L.A., and Haystead, T.A. (2012). A highly selective Hsp90 affinity chromatography resin with a cleavable linker. *Bioorg. Med. Chem.* 20, 3298–3305.
- Ide, M., and Suzuki, Y. (2005). Is whole-body FDG-PET valuable for health screening? *For. Eur. J. Nucl. Med. Mol. Imaging* 32, 339–341.
- Kamal, A., Thao, L., Sensintaffar, J., Zhang, L., Boehm, M.F., Fritz, L.C., and Burrows, F.J. (2003). A high-affinity conformation of Hsp90 confers tumour selectivity on Hsp90 inhibitors. *Nature* 425, 407–410.

- Kim, Y.S., Alarcon, S.V., Lee, S., Lee, M.J., Giaccone, G., Neckers, L., and Trepel, J.B. (2009). Update on Hsp90 inhibitors in clinical trial. *Curr. Top. Med. Chem.* 9, 1479–1492.
- Koga, F., Kihara, K., and Neckers, L. (2009). Inhibition of cancer invasion and metastasis by targeting the molecular chaperone heat-shock protein 90. *Anticancer Res.* 29, 797–807.
- Liu, C., Rajaram, N., Vishwanath, K., Jiang, T., Palmer, G.M., and Ramanujam, N. (2012). Experimental validation of an inverse fluorescence Monte Carlo model to extract concentrations of metabolically relevant fluorophores from turbid phantoms and a murine tumor model. *J. Biomed. Opt.* 17, 077012.
- McCready, J., Sims, J.D., Chan, D., and Jay, D.G. (2010). Secretion of extracellular hsp90alpha via exosomes increases cancer cell motility: a role for plasminogen activation. *BMC Cancer* 10, 294.
- Mollapour, M., and Neckers, L. (2012). Post-translational modifications of Hsp90 and their contributions to chaperone regulation. *Biochim. Biophys. Acta* 1823, 648–655.
- Moulick, K., Ahn, J.H., Zong, H., Rodina, A., Cerchietti, L., Gomes DaGama, E.M., Caldas-Lopes, E., Beebe, K., Perna, F., Hatzl, K., et al. (2011). Affinity-based proteomics reveal cancer-specific networks coordinated by Hsp90. *Nat. Chem. Biol.* 7, 818–826.
- Neckers, L., and Workman, P. (2012). Hsp90 molecular chaperone inhibitors: are we there yet? *Clin. Cancer Res.* 18, 64–76.
- Neckers, L., Mollapour, M., and Tsutsumi, S. (2009). The complex dance of the molecular chaperone Hsp90. *Trends Biochem. Sci.* 34, 223–226.
- Neve, R.M., Chin, K., Fridlyand, J., Yeh, J., Baehner, F.L., Fevr, T., Clark, L., Bayani, N., Coppe, J.P., Tong, F., et al. (2006). A collection of breast cancer cell lines for the study of functionally distinct cancer subtypes. *Cancer Cell* 10, 515–527.
- Palmer, G.M., and Ramanujam, N. (2008). Monte-Carlo-based model for the extraction of intrinsic fluorescence from turbid media. *J. Biomed. Opt.* 13, 024017.
- Palmer, G.M., Boruta, R.J., Viglianti, B.L., Lan, L., Spasojevic, I., and Dewhirst, M.W. (2010). Non-invasive monitoring of intra-tumor drug concentration and therapeutic response using optical spectroscopy. *J. Control. Release* 142, 457–464.
- Pick, E., Kluger, Y., Giltman, J.M., Moeder, C., Camp, R.L., Rimm, D.L., and Kluger, H.M. (2007). High HSP90 expression is associated with decreased survival in breast cancer. *Cancer Res.* 67, 2932–2937.
- Ray, R., and Haystead, T.A. (2003). Phosphoproteome analysis in yeast. *Methods Enzymol.* 366, 95–103.
- Samant, R.S., Clarke, P.A., and Workman, P. (2012). The expanding proteome of the molecular chaperone HSP90. *Cell Cycle* 11, 1301–1308.
- Schoder, H., and Gonen, M. (2007). Screening for cancer with PET and PET/CT: potential and limitations. *J. Nucl. Med.* 48(Suppl 1), 4S–18S.
- Sidera, K., El Hamidieh, A., Mamalaki, A., and Patsavoudi, E. (2011). The 4C5 cell-impermeable anti-HSP90 antibody with anti-cancer activity, is composed of a single light chain dimer. *PLoS ONE* 6, e23906.
- Sims, J.D., McCready, J., and Jay, D.G. (2011). Extracellular heat shock protein (Hsp)70 and Hsp90 $\alpha$  assist in matrix metalloproteinase-2 activation and breast cancer cell migration and invasion. *PLoS ONE* 6, e18848.
- Smith, R.A., Cokkinides, V., Brooks, D., Saslow, D., and Brawley, O.W. (2010). Cancer screening in the United States, 2010: a review of current American Cancer Society guidelines and issues in cancer screening. *CA Cancer J. Clin.* 60, 99–119.
- Stellas, D., El Hamidieh, A., and Patsavoudi, E. (2010). Monoclonal antibody 4C5 prevents activation of MMP2 and MMP9 by disrupting their interaction with extracellular HSP90 and inhibits formation of metastatic breast cancer cell deposits. *BMC Cell Biol.* 11, 51.
- Trepel, J., Mollapour, M., Giaccone, G., and Neckers, L. (2010). Targeting the dynamic HSP90 complex in cancer. *Nat. Rev. Cancer* 10, 537–549.
- Tsutsumi, S., and Neckers, L. (2007). Extracellular heat shock protein 90: a role for a molecular chaperone in cell motility and cancer metastasis. *Cancer Sci.* 98, 1536–1539.
- Tsutsumi, S., Scroggins, B., Koga, F., Lee, M.J., Trepel, J., Felts, S., Carreras, C., and Neckers, L. (2008). A small molecule cell-impermeant Hsp90 antagonist inhibits tumor cell motility and invasion. *Oncogene* 27, 2478–2487.
- Tsutsumi, S., Mollapour, M., Graf, C., Lee, C.T., Scroggins, B.T., Xu, W., Haslerova, L., Hessling, M., Konstantinova, A.A., Trepel, J.B., et al. (2009). Hsp90 charged-linker truncation reverses the functional consequences of weakened hydrophobic contacts in the N domain. *Nat. Struct. Mol. Biol.* 16, 1141–1147.
- Vaughan, C.K., Neckers, L., and Piper, P.W. (2010). Understanding of the Hsp90 molecular chaperone reaches new heights. *Nat. Struct. Mol. Biol.* 17, 1400–1404.
- Wang, X., Song, X., Zhuo, W., Fu, Y., Shi, H., Liang, Y., Tong, M., Chang, G., and Luo, Y. (2009). The regulatory mechanism of Hsp90alpha secretion and its function in tumor malignancy. *Proc. Natl. Acad. Sci. USA* 106, 21288–21293.
- Wang, Y., Trepel, J.B., Neckers, L.M., and Giaccone, G. (2010). STA-9090, a small-molecule Hsp90 inhibitor for the potential treatment of cancer. *Curr. Opin. Investig. Drugs* 11, 1466–1476.
- Warning, K., Hildebrandt, M.G., Kristensen, B., and Ewertz, M. (2011). Utility of 18FDG-PET/CT in breast cancer diagnostics—a systematic review. *Dan. Med. Bull.* 58, A4289.
- Whitesell, L., and Lindquist, S.L. (2005). HSP90 and the chaperoning of cancer. *Nat. Rev. Cancer* 5, 761–772.
- Xu, W., Yuan, X., Xiang, Z., Mimnaugh, E., Marcu, M., and Neckers, L. (2005). Surface charge and hydrophobicity determine ErbB2 binding to the Hsp90 chaperone complex. *Nat. Struct. Mol. Biol.* 12, 120–126.
- Yin, X., Zhang, H., Lundgren, K., Wilson, L., Burrows, F., and Shores, C.G. (2010). BIIB021, a novel Hsp90 inhibitor, sensitizes head and neck squamous cell carcinoma to radiotherapy. *Int. J. Cancer* 126, 1216–1225.
- Zhou, D., Liu, T.F., Ye, Y., Ying, J., Shin, W., Ogawa, L., Inoue, T., Lee, W., Adjiri-Awore, A., Kolodzieyski, L., et al. (2012). Associating retinal drug exposure and retention with the ocular toxicity profiles of Hsp90 inhibitors. *J. Clin. Oncol.* 30, (suppl; abstr 3086).